

Note on the use of Yee-lattices in (semi-) implicit Particle-in-cell codes

Andreas Kempf, Urs Ganse, Patrick Kilian, Felix Spanier

*Lehrstuhl für Astronomie, Universität Würzburg, Emil-Fischer-Straße 31, D-97074
Würzburg*

Abstract

A modification of the implicit algorithm for particle-in-cell simulations proposed by Petrov and Davis [1] is presented. The original lattice arrangement is not inherently divergence-free, possibly leading to unphysical results. This arrangement is replaced by a staggered mesh resulting in a reduction of the divergence of the magnetic field by several orders of magnitude.

Keywords:

particle in cell, divergence, Yee, implicit timestep

1. Introduction

In order to correctly reproduce physical processes in a particle-in-cell code, Maxwell's equations need to be solved consistently. However, the requirement of the magnetic field being divergence free is often violated by numerical algorithms leading to unphysical results [2]. Consequently, several divergence-cleaning schemes have been proposed, providing a way to remove magnetic source terms after the fact. Another possibility to correctly incorporate Gauss' law for magnetism into a PiC-code is to use the staggered mesh first proposed by Yee [3] in 1966. The special arrangement of electric and magnetic fields inherently conserves a zero-valued divergence [4], provided that $\nabla \cdot \vec{B} = 0$ at $t = 0$. A comparison by Balsara and Kim [5] identifies several problems of divergence-cleaning methods in MHD and notes their absence when using a staggered mesh.

Email address: akempf@astro.uni-wuerzburg.de (Andreas Kempf)

Petrov and Davis [1] proposed an implicit particle-in-cell algorithm forgoing the staggered mesh approach. Continuing previous work by Kilian et al. [6] we intend to use this algorithm to study particle acceleration in astrophysical plasmas while keeping unphysical effects to a minimum. In this paper we therefore modify the scheme, incorporating the Yee lattice and effecting a reduction of $\nabla \cdot \vec{B}$ by several orders of magnitude.

2. Definitions

The quantities from [1] that are relevant to this paper are

$$\hat{S}_\alpha^{n+1/2} = \frac{n_\alpha q_\alpha}{4\epsilon_0 m_\alpha \gamma_\alpha^{n+1/2}} \hat{T}_\alpha^{n+1/2} \quad (1)$$

and

$$\delta \vec{j}_\alpha^{n+1/2} = \frac{n_\alpha q_\alpha}{2m_\alpha \gamma_\alpha^{n+1/2}} \left(\vec{p}_\alpha^n + \hat{T}_\alpha^{n+1/2} \left(\vec{p}_\alpha^n \times \Delta \vec{\Omega}_\alpha^{n+1/2} \right) \right). \quad (2)$$

The tensor \hat{T} (with indices suppressed for brevity) is defined as

$$\hat{T} = \frac{1}{1 + |\Delta \vec{\Omega}|^2} \begin{bmatrix} 1 + \Delta \Omega_x^2 & \Delta \Omega_x \Delta \Omega_y + \Delta \Omega_z & \Delta \Omega_x \Delta \Omega_z - \Delta \Omega_y \\ \Delta \Omega_x \Delta \Omega_y - \Delta \Omega_z & 1 + \Delta \Omega_y^2 & \Delta \Omega_y \Delta \Omega_z + \Delta \Omega_x \\ \Delta \Omega_x \Delta \Omega_z + \Delta \Omega_y & \Delta \Omega_y \Delta \Omega_z - \Delta \Omega_x & 1 + \Delta \Omega_z^2 \end{bmatrix} \quad (3)$$

with

$$\Delta \vec{\Omega}_\alpha^{n+1/2} = \frac{q_\alpha \vec{B}_\alpha^{n+1/2}}{m_\alpha \gamma_\alpha^{n+1/2}} \frac{\Delta t}{2}. \quad (4)$$

The quantities q_α , m_α , n_α are the charge, mass, and number density of (computational) particle α . $\gamma_\alpha^{n+1/2}$ is the particle's relativistic gamma factor and $\vec{B}_\alpha^{n+1/2}$ its local magnetic field at time $n + 1/2$. \vec{p}_α^n is the momentum of particle α at time n .

The deposition of \hat{S} and $\delta \vec{j}$ on the grid and the interpolation of \vec{E} and \vec{B} to the particle position is achieved via a standard weighting function. Our algorithm makes use of the triangular shaped cloud (TSC) scheme.

3. The modified lattice arrangement

The original algorithm by Petrov and Davis [1] stores electric fields on grid nodes and magnetic fields in the cell center. The vector quantity $\delta \vec{j}$ and

the tensor quantity \hat{S} are deposited on grid nodes, as well. Since the electric field is updated according to

$$\left(\hat{\mathbf{I}} + \hat{S}^{n+1/2}\right) \vec{E}^{n+1} = \left(\hat{\mathbf{I}} - \hat{S}^{n+1/2}\right) \vec{E}^n + \frac{\Delta t}{\varepsilon_0} \left(\vec{\nabla} \times \vec{H}^{n+1/2} - \delta \vec{j}^{n+1/2}\right), \quad (5)$$

and all required quantities are defined on grid nodes, this equation can be solved locally for \vec{E}^{n+1} .

Our approach keeps the original field layout by Yee [3] with the components of $\delta \vec{j}$ stored like the corresponding components of the electric field. \hat{S} is stored on grid nodes and interpolated linearly for each component of the electric field to be calculated. When calculating the new value for $E_x^{i+1/2,j,k}$, \hat{S} is taken to be $(\hat{S}^{i,j,k} + \hat{S}^{i+1,j,k})/2$, for $E_y^{i,j+1/2,k}$ it is $(\hat{S}^{i,j,k} + \hat{S}^{i,j+1,k})/2$ and for $E_z^{i,j,k+1/2}$ it is $(\hat{S}^{i,j,k} + \hat{S}^{i,j,k+1})/2$.

Since \hat{S} is not a diagonal tensor, all the components of $\delta \vec{j}$, $\nabla \times \vec{B}$ and \vec{E}^n need to be known at the same point as the component of \vec{E}^{n+1} to be calculated, as well. These three quantities can be interpolated the same way.

For E_x^{n+1} :

$$A_x^{i+1/2,j,k} = A_x^{i+1/2,j,k} \quad (6)$$

$$A_y^{i+1/2,j,k} = (A_y^{i,j+1/2,k} + A_y^{i,j-1/2,k} + A_y^{i+1,j+1/2,k} + A_y^{i+1,j-1/2,k}) / 4 \quad (7)$$

$$A_z^{i+1/2,j,k} = (A_z^{i,j,k+1/2} + A_z^{i,j,k-1/2} + A_z^{i+1,j,k+1/2} + A_z^{i+1,j,k-1/2}) / 4 \quad (8)$$

For E_y^{n+1} :

$$A_x^{i,j+1/2,k} = (A_x^{i+1/2,j,k} + A_x^{i+1/2,j+1,k} + A_x^{i-1/2,j,k} + A_x^{i-1/2,j+1,k}) / 4 \quad (9)$$

$$A_y^{i,j+1/2,k} = A_y^{i,j+1/2,k} \quad (10)$$

$$A_z^{i,j+1/2,k} = (A_z^{i,j,k+1/2} + A_z^{i,j+1,k+1/2} + A_z^{i,j,k-1/2} + A_z^{i,j+1,k-1/2}) / 4 \quad (11)$$

For E_z^{n+1} :

$$A_x^{i,j,k+1/2} = (A_x^{i+1/2,j,k} + A_x^{i+1/2,j,k+1} + A_x^{i-1/2,j,k} + A_x^{i-1/2,j,k+1}) / 4 \quad (12)$$

$$A_y^{i,j,k+1/2} = (A_y^{i,j+1/2,k} + A_y^{i,j+1/2,k+1} + A_y^{i,j-1/2,k} + A_y^{i,j-1/2,k+1}) / 4 \quad (13)$$

$$A_z^{i,j,k+1/2} = A_z^{i,j,k+1/2} \quad (14)$$

4. Simulation setup

In order to compare the original lattice configuration with the Yee lattice, identical simulations are performed using both algorithms.

electron plasma frequency	ω_{pe}	$2.0 \cdot 10^8$ rad/s
length of timestep	Δt	$4.1 \cdot 10^{-10}$ s
Debye length	λ_D	7.5 cm
cell edge length	Δx	21 cm
mass ratio	m_p/m_e	42

Table 1: Parameters of the thermal plasma.

The size of the three-dimensional lattice is $64 \times 64 \times 64$ with periodic boundary conditions. There are 25 electrons and 25 protons in each cell. Each simulation is running for 4000 timesteps. The plasma is chosen to be thermal, meaning that the velocity components for each particle are independent and follow a Gaussian distribution of width v_{th} . The protons and electrons are in thermal equilibrium so that the width of the Gaussian distribution of the protons is equal to v_{th} divided by the square root of the mass ratio $\sqrt{m_p/m_e}$.

The physical parameters are listed in table 1.

5. Results

When directly comparing $\nabla \cdot \vec{B}$ at the end of the two simulation runs, a significant difference is manifest. The ratio of the total divergence of both simulations at timestep 4000 is

$$\frac{\sum_{ijk} |\nabla \cdot \vec{B}_{Yee}|}{\sum_{ijk} |\nabla \cdot \vec{B}_{original}|} = 7.6 \cdot 10^{-15} \quad (15)$$

Fourier transforming $\nabla \cdot \vec{B}$ at timestep 4000 in space and plotting the absolute values for a slice along the z-axis yields figure 1. As can be seen, the original arrangement introduces high-amplitude patterns at short wavelengths. The Yee-arrangement mostly produces low-amplitude noise, as desired.

Furthermore, plots of the y-component of the magnetic field, prepared the same way, are shown in figure 2. The original lattice arrangement introduces unphysical behavior at short wavelengths which is not present when using a Yee-lattice.

A dispersion plot of the y-component of the electric field along the x-axis for the simulation using the Yee-lattice is obtained as follows. For each timestep the E_y values are summed up for slices perpendicular to the x-axis.

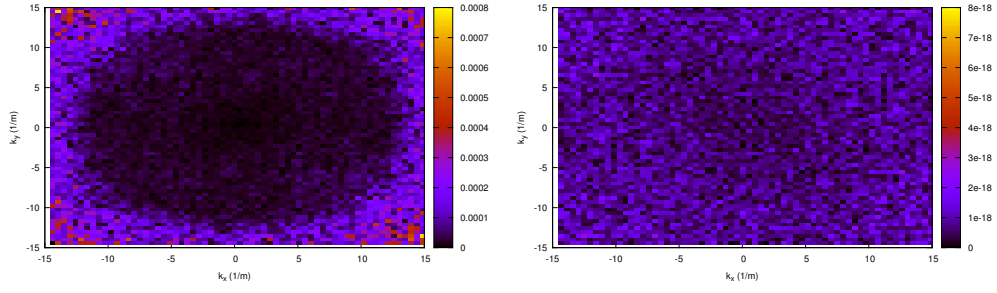


Figure 1: Spectral plot of the distribution of $\nabla \cdot \vec{B}$ in x- and y-direction for the original lattice arrangement (left) and the Yee arrangement (right).

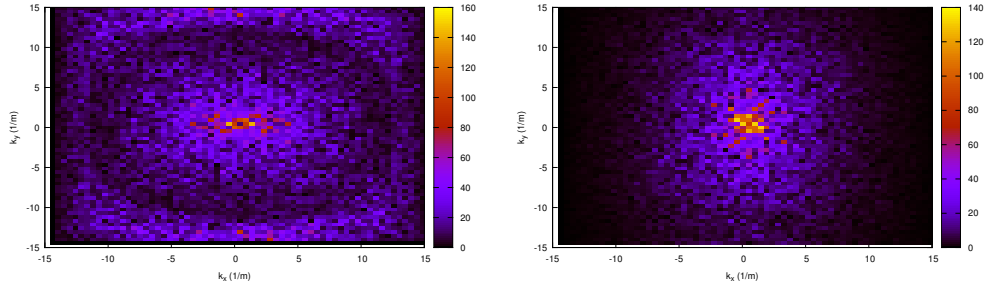


Figure 2: Spectral plot of the distribution of B_y in x- and y-direction for the original lattice arrangement (left) and the Yee arrangement (right).

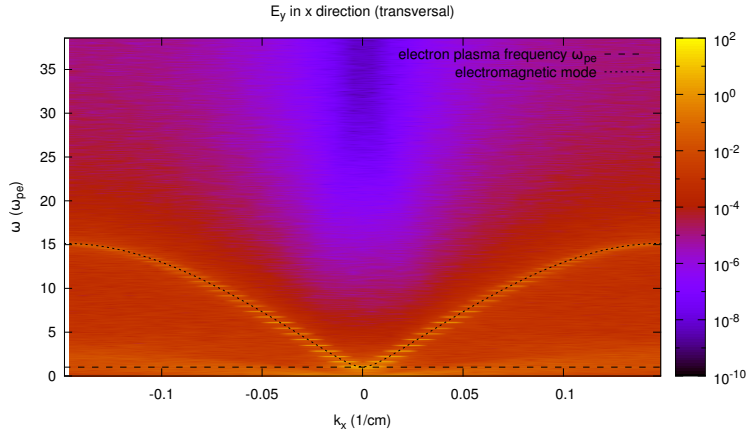


Figure 3: Plot of the dispersion relation of E_y along the x-axis. The expected dispersion of the electromagnetic wave, incorporating numerical effects, is also shown.

A Fourier transformation in space and time results in a ω - k_x relation, depicted in figure 3. In addition, the dispersion of the electromagnetic wave as predicted by theoretical calculations is shown (incorporating effects from finite Δt and Δx). As can be seen, the modified code correctly describes wave dispersion in a thermal plasma indicating that the alterations do not introduce unphysical effects. Likewise, further tests of more complicated simulation setups do not show unexpected behavior resulting from our changes.

Finally, the simulations are repeated with Δx and Δt scaled down by a factor of 4, permitting a comparison with our explicit PiC Code ACRONYM [6]. The energy development for the implicit scheme using the Yee-lattice, the explicit scheme, and the unaltered implicit scheme are shown in figure 4. The original scheme shows deviations from the explicit results with the magnetic field energy growing steadily over the course of the simulation. In contrast, the altered scheme nicely reproduces the energy development of the ACRONYM simulation.

As shown, it is possible to alter the algorithm proposed by Petrov and Davis [1] to obtain a divergence-free setup. In our code, the only steps that needed to be modified were the deposition and interpolation of grid quantities and the calculation of the updated fields. The former change is easily implemented by adjusting the offsets used when evaluating the weighting function. The latter change is described in section 3.

Due to the additional calculations introduced into the scheme, some per-

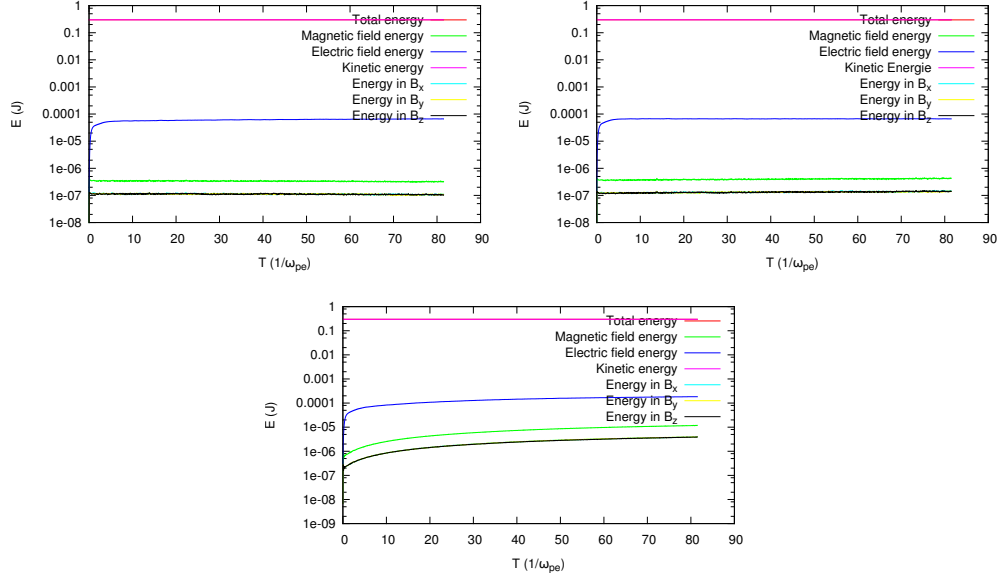


Figure 4: Energy development of the rescaled thermal simulation for the altered implicit scheme (top left), the explicit scheme used in ACRONYM (top right) and the original scheme (bottom).

formance is lost. However, since most of the changes are confined to the field update step which only needs to be executed once per cell and timestep, the performance loss is small and on the order of a few percent.

References

- [1] G. M. Petrov, J. Davis, A generalized implicit algorithm for multi-dimensional particle-in-cell simulations in cartesian geometry, *Physics of Plasmas* 18 (2011) 073102.
- [2] J. Brackbill, D. Barnes, The effect of nonzero $\nabla \cdot B$ on the numerical solution of the magnetohydrodynamic equations, *Journal of Computational Physics* 35 (1980) 426 – 430.
- [3] K. Yee, Numerical solution of initial boundary value problems involving maxwell’s equations in isotropic media, *Antennas and Propagation, IEEE Transactions on* 14 (1966) 302 –307.

- [4] A. Tafflove, S. C. Hagness, Computational Electrodynamics: The Finite-Difference Time-Domain Method, Artech House, Norwood, 2nd edition, 2000.
- [5] D. S. Balsara, J. Kim, A comparison between divergence-cleaning and staggered-mesh formulations for numerical magnetohydrodynamics, The Astrophysical Journal 602 (2004) 1079.
- [6] P. Kilian, T. Burkart, F. Spanier, The influence of the mass ratio on particle acceleration by the filamentation instability, in: W. E. Nagel, D. B. Kröner, M. M. Resch (Eds.), High Performance Computing in Science and Engineering '11, Springer, Berlin Heidelberg, 2012, pp. 5–13.